# ANALYSIS OF FIELD OBSERVATION DATA TO DEVELOP PERFORMANCE REQUIREMENTS FOR LIVING SNOW FENCES DURING SEVERE SNOWSTORM EVENTS

Yusuke Harada[1]*, Akihiro Yoshii[1], Satoshi Omiya[1] and Atsushi Nishimura[1]

[1] *Civil Engineering Research Institute for Cold Region, Public Works Research Institute, Sapporo, Japan*

ABSTRACT: We conducted observations on trees and meteorological elements related to blowing snow using shelterbelts composed of evergreen conifers to investigate a method for designing living snow fences against severe snowstorm events. These observations were done during the 2022/23 and 2023/24 winters in a snowy, windy area of northern Japan. We analyzed the field observation data and created benchmark data based on the cumulative plant area density's relationship with the ratio of leeward wind speed to windward wind speed and with the ratio of leeward snow mass flux to windward snow mass flux, in order to consider the calculation conditions for the numerical simulation of blowing and drifting snow.

KEYWORDS: living snow fences, severe snowstorm events, performance requirements

## 1. INTRODUCTION

In recent years, the cold snowy regions of Japan have tended to see more incidents of vehicles being stuck in snow and roads being closed due to severe snowstorms caused by rapidly developing low-pressure systems and convergence zones. Living snow fences (LSFs) have been installed since 1976 along roads in Hokkaido, northern Japan, to mitigate blowing snow, and these have reduced road traffic problems, such as snowdrifts and poor visibility (CERI, 2011). LSFs in Hokkaido totaled approximately 100 km as of 2020 (Sakurai et al., 2023). "The Highway Snowstorm Countermeasure Manual" sets three standard widths (10 m, 20 m, and 30 m) for LSFs on national highways whose maximum snowdrift volume is 20 $m^3$ $m^{-1}$ or greater, based on experience in Japan (CERI, 2011). However, there are no established methods for designing LSFs to meet the performance required for severe snowstorm events in Japan. Therefore, we conducted observations on trees and meteorological elements related to blowing snow using shelterbelts composed of evergreen conifers to investigate a method for designing LSFs against severe snowstorm events during the 2022/23 and 2023/24 winters in a snowy, windy area of northern Japan. Next, we analyzed the field observation data and created benchmark data based on the cumulative plant area density's relationship with the ratio of leeward wind speed to windward wind speed (hereinafter: the wind speed ratio) and with the ratio of leeward snow mass flux to windward snow mass flux (hereinafter: the snow mass flux ratio), in order to consider the calculation conditions for numerical simulations of blowing and drifting snow. The goal is to present an optimized configuration for LSFs that can meet the performance required for severe snowstorm events.

* *Corresponding author address:*
Yusuke Harada, Civil Engineering Research Institute for Cold Region, PWRI, 1-3-1-34 Hiragishi, Toyohira-ku, Sapporo, Hokkaido 062-8602;
tel: +81-11-841-1746; fax: +81-11-841-9747;
email: harada-y@ceri.go.jp

## 2. OBSERVATION METHODS

### *2.1 Study site*

The study site was the Ishikari Blowing Snow Test Field of the Civil Engineering Research Institute for Cold Region in southwestern Hokkaido, northern Japan (N43°12', E141°23'). At the times of blowing snow at the field, the prevailing winds were from compass directions ranging from W to NNW. We carried out observations on trees and meteorological elements related to blowing snow in order to investigate a design methodology. We set two observation sites: Site A and Site B. Site A was a linear shelterbelt of approximately 80 m long by 15-30 m wide consisting mainly of Pinaceae, oriented N–S in the field and used in the 2022/23 and 2023/24 winters. At this site, three survey lines were set (oriented E–W; A-1 to A-3) orthogonal to the shelterbelt (Figure 1).

Along survey line 1, we removed the lower branches to an average height of 2 m before the 2023/24 winter season. The area where the lower branches were removed is indicated by the dotted line in the upper right area of Figure 1. On 30 January 2024, a 2-m-high by 15-m-long auxiliary fence covered with windbreak netting with a void ratio of 50% was installed inside the tree zone 8.6 m from the line that connected the starting points of the three survey lines. The windbreak netting (50% void ratio) was replaced by a vinyl sheet

(0% void ratio) on 28 February 2024. At Site B, observations on the state of the trees and fixed-point observations of weather were conducted in an area of about 90 m by 10 m to 20 m (oriented E–W) that mainly consisted of Pinaceae species (evergreen conifers) during the 2023/24 winter. At this site, four survey lines (B-1 to B-4, oriented NNW–SSE) were set to gather data on snow blowing from the NNW (Figure 1).

### 2.2 *Tree observation*

We conducted tree observations to determine the structure and plant area density (PAD) of the shelterbelt using a drone equipped with LiDAR and a camera (DJI Matricce 300 RTK and Zemuse L1). We acquired point cloud data and images from an area approximately 80 m by 80 m at Site A on 2 December 2022 and 9 May 2024 (after the lower branches around the A-1 line had been cut) and at Site B on 9 May 2024. The LiDAR measurements were taken under three angle conditions: vertical downward (0°), oblique (45°), and lateral (60°) using iterative and non-iterative scanning (Figure 1, lower left). Using the raw scan data, point cloud data (3D XYZ data) were generated in LAS format using DJI Terra software. The LAS data, including precipitation particles, were manually cleaned up using point cloud editing software (CloudCompare). Using camera images with a wrap rate of 80%, an orthoimage (GeoTIFF) of the observation area was created using the Structure-from-Motion/Multi-View-Stereo (SfM–MVS) method.

Tree surveys were conducted to acquire tree height, diameter at breast height, crown width, crown base height, and the lower limit height of dead branches. 65 conifers were surveyed by the belt transect method (width = 10 m) using lines A-1 to A-3 before the 2022/23 winter at Site A. Also, 27 conifers were surveyed in Site B after the 2023/24 winter (see Figures 2 and 3).

### 2.3 *Meteorological observation*

Meteorological observations were conducted during the 2022/23 and 2023/24 winters at Site A and during the 2023/24 winter at Site B. The measured elements were the mass flux of blowing snow measured using snow particle counters (SPC-95) and the wind speed and direction measured using propeller-vane anemometers (KDC-S04). Sensors were set at one point windward and three points leeward of the shelterbelt at a height of 1.8 m at Site A, and at one point windward and four points leeward of the shelterbelt at a height of 1.8 m at Site B. The measurement interval was 1 minute for the wind speed and direction and 1 second for the mass flux of blowing snow. These data were organized as 10-minute statistics. Here, the wind speed was the average value, the wind direction was the mode value, and the mass flux of blowing snow was the cumulative value. In addition, the air temperature was measured using a platinum resistance thermometer, and snowfall converted to the precipitation rate (mm $h^{-1}$) was measured using a double fence intercomparison reference (DFIR: Goodison et al., 1998) in the test field. These data were organized as 10-minute statistics. Here, the air temperature is the average value, and the snowfall converted to the precipitation rate is the difference between the current snowfall and the snowfall from 10 minutes earlier. The measurement periods and elements for Site A and Site B are shown in Table 1.

## 3. RESULTS AND ANALYSIS

To understand how the elements of evergreen coniferous tree belts and auxiliary fences affect the snow control performance (expressed as the wind speed ratio and the snow mass flux ratio), we compiled and analyzed the results of the tree observations (i.e., the results of the unmanned aerial vehicle (UAV) measurements and the field tree surveys) and the results of the meteorological observations. In considering the creation of benchmark data that show the snow control performance of LSFs during blowing snow, we focused on the items below for the observation points on the windward side.

- Wind direction: W (Site A), NNW (Site B)
- Wind speed (at the height of 1.8 m): 5 m $s^{-1}$ or higher (wind speed ratio), 3 m $s^{-1}$ or higher (snow mass flux ratio)
- Air temperature: 0°C or lower (snow mass flux ratio)
- Snow mass flux (at a height of 1.8 m): greater than 0 g $m^{-2}$ $s^{-1}$ (snow mass flux ratio)

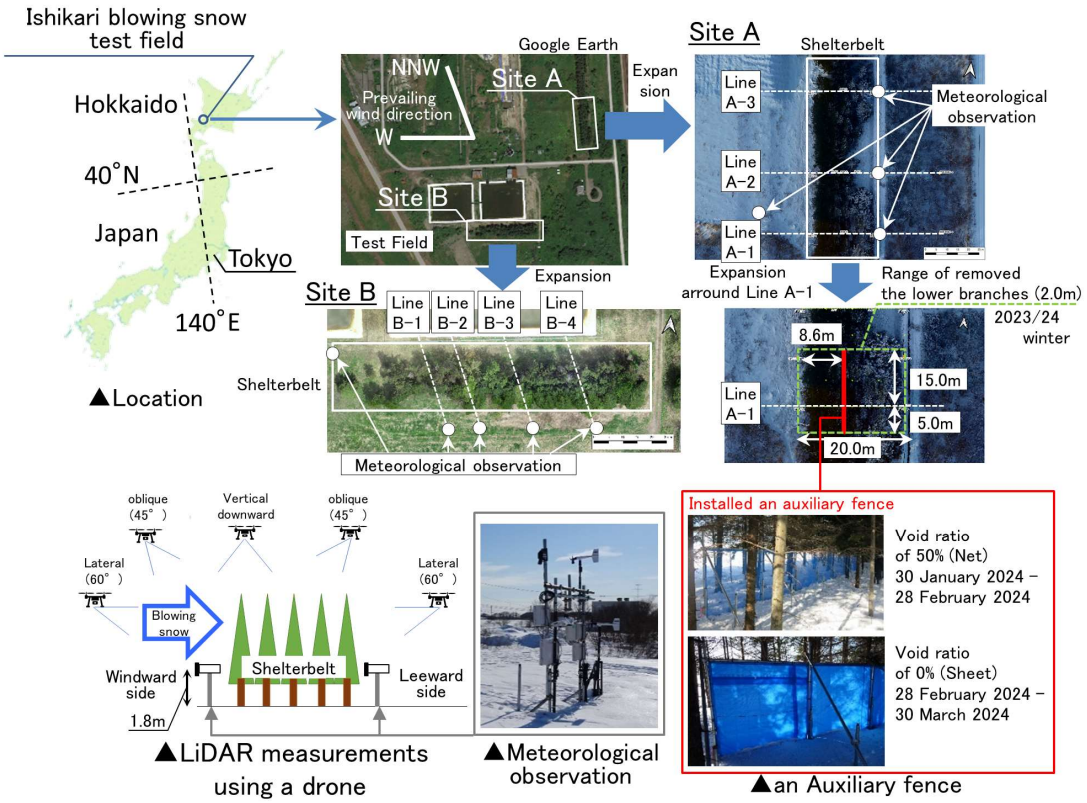


Figure 1: Description of the study site.

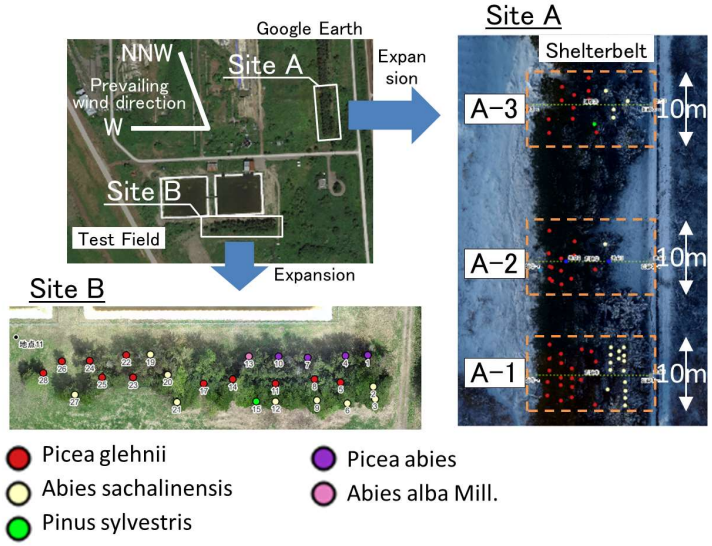


Figure 2: The belt transect ranges (the orange dotted line), and positions of tree survey (color points).

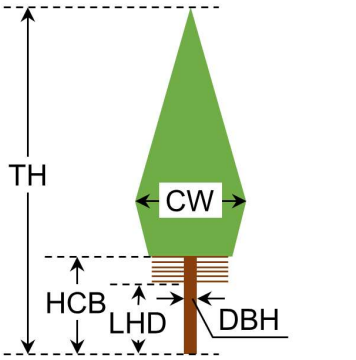


Figure 3: Items of tree survey.

Table 1: Observation duration and observed elements at sites A and B.

| | | Site A | | Site B |
|---|---|---|---|---|
| | | 2022/23 winter | 2023/24 winter | 2023/24 winter |
| Period | Start | 10 December 2022 | 1 December 2023 | 1 December 2023 |
| | End | 9 March 2023 | 30 March 2024 | 21 January 2024 |
| Elements | Sites | - Wind speed and direction<br>- Snow mass flux | - Wind speed and direction | - Wind speed and direction |
| | Test field etc. | - Snowfall converted to the precipitation rate<br>- Air temperature | | |

### 3.1 *Calculation of PAD at the height of meteorological observation*

We determined the cross sectional distribution (1-m-grid resolution) of PAD values for each survey line by using the point cloud data obtained from non-iterative UAV measurements in the vertical downward direction. We used lidR library of the statistical software R, which utilizes the method of Bouvier et al. (2015) (the upper subfigures in Figure 4). lidR is software that models the attenuation of a laser irradiated downward from a location over the target until it reaches the interior of the target. We compared the results of the PAD cross sectional distribution with the point cloud data for the survey lines combining the vertical downward (0°), oblique (45°), and lateral (60°) measurement profiles, shown in the lower subfigures in Figure 4 (Harada et al. (2023)). The crown base height (HCB, see Figure 3) was generally expressed well for all survey lines. Through this comparison, we confirmed the validity of the presentation of lidR using the PAD cross sectional distribution. Table 2 shows the cumulative PAD value (ΣPAD) and the average PAD value (PAD_Avg.) for each survey line. Here, the PAD at a height of 1.8 m was taken as the average of the PAD grid values for the heights of 1 to 3 m (see upper subfigures in Figure 4).

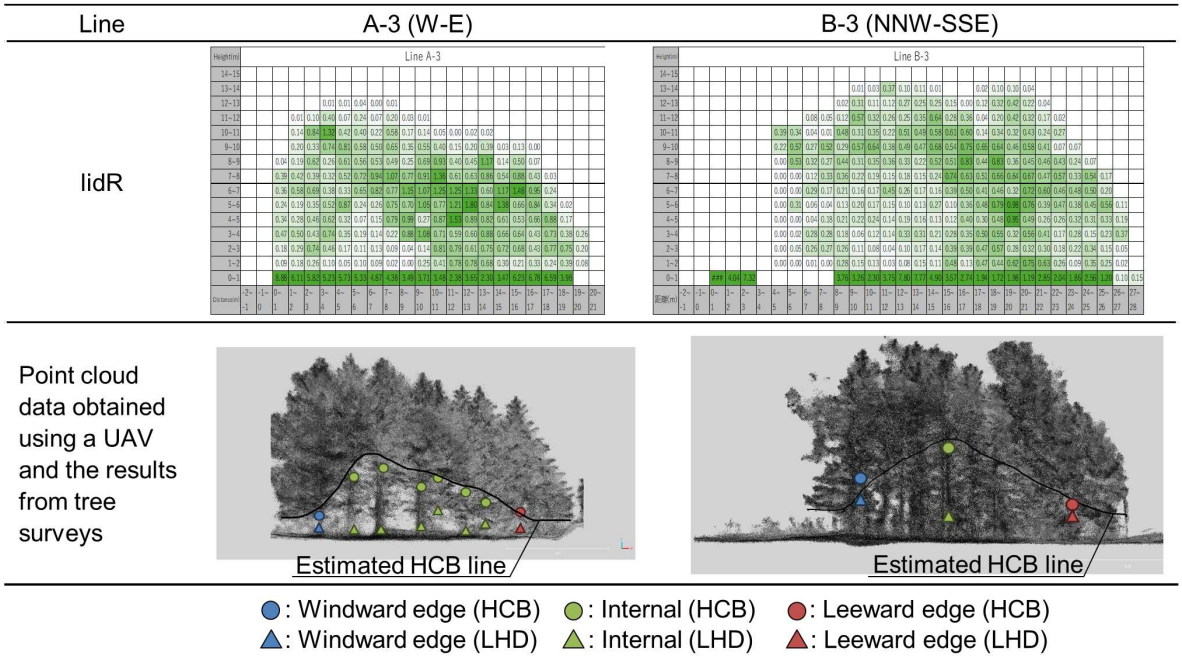


Figure 4: PAD distribution by lidR along survey lines A-3 and B-4 (1-m-grid resolution). Comparison between the point cloud data obtained using a UAV and the results from tree surveys.

Table 2: ΣPAD and PAD_Avg. values for each survey line.

| | | ΣPAD ($m^2$ $m^{-1}$) | | PAD_Ave. ($m^2$ $m^{-2}$) | |
|---|---|---|---|---|---|
| Line | Range | All | 1.8 m height | All | 1.8 m height |
| A-1 | Before* | 100.64 | 12.70 | 0.50 | 0.33 |
| A-1 | After* | 103.27 | 8.38 | 0.52 | 0.20 |
| A-2 | | 67.06 | 13.96 | 0.50 | 0.47 |
| A-3 | | 97.09 | 14.68 | 0.49 | 0.35 |
| B-1 | | 69.13 | 13.56 | 0.33 | 0.35 |
| B-2 | | 83.59 | 18.85 | 0.30 | 0.38 |
| B-3 | | 77.08 | 10.58 | 0.30 | 0.23 |
| B-4 | | 92.48 | 10.49 | 0.32 | 0.21 |

Before*: Before the lower branches were removed, After*: After the lower branches were removed

### 3.2 Tree and meteorological observation data

The ratio of leeward wind speed to windward wind speed and that of leeward snow mass flux to windward snow mass flux for Site A and Site B obtained from meteorological observations are shown in Figures 5 and 6, together with tree observation results and the elements obtained in Section 3.1. Note that the wind speed and the wind speed ratio (survey lines A-2 and B-1) increase with increase in the distance of the measurement point from the leeward edge of the shelterbelt. The tree observation elements that were found to be related to both the wind speed ratio and the snow mass flux ratio were the shelterbelt width and the ΣPAD at a height of 1.8 m. Note that before the removal of the lower branches (hereinafter: pruning), the wind speed ratio differed between survey lines A-3 and A-1, which have the same shelterbelt width (19 m), and it is assumed that in addition to ΣPAD affecting the wind speed ratio, the height of crown base (HCB) and the lower limit height of dead branches (LHD) also affect that ratio (see Figure 3). Additionally, based on the wind speed ratio at survey line A-1 being greater after pruning, we confirmed that the amount of branches and leaves in the area where pruning was done affects the wind speed ratio. Regarding the effectiveness of the auxiliary fence at survey line A-1, the wind speed ratio for the fence with a void ratio of 0% was lower than that for the fence with a void ratio of 50%, and the wind speed ratio for the auxiliary fence with a void ratio of 0% was about the same as that before pruning (Figure 5).

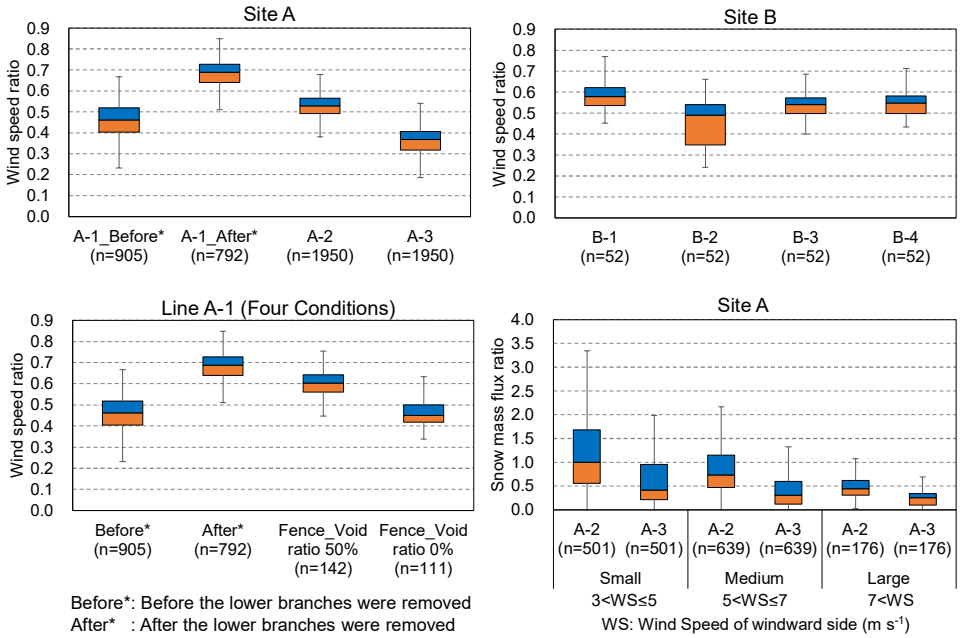


Figure 5: Ratio of leeward wind speed to windward wind speed and of leeward snow mass flux to windward snow mass flux for sites A and B. The distance between the edge of the tree belt and the measuring equipment: Site A: survey line A-2: 5 m, survey lines 1 and 3: 1 m; Site B: survey line B-1: 14 m, other survey lines: 8 m. Note: Outliers are not plotted in the box-and-whisker diagram.

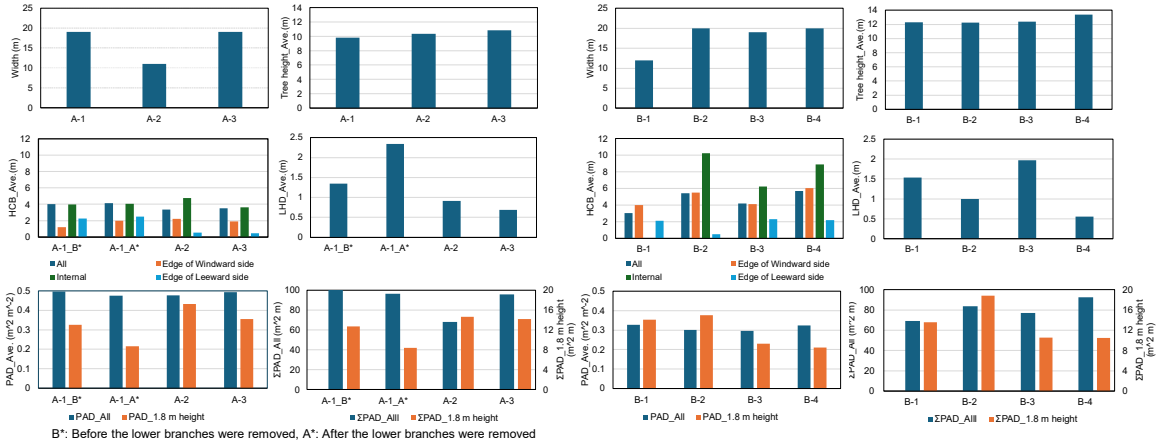


Figure 6: Results of tree observations and elements affecting PAD.

### 3.3 *Creation of benchmark data*

Based on the results of Section 3.2, we created a set of benchmark data with which to consider the calculation conditions for numerical simulations of blowing and drifting snow. The benchmark data consisted of performance indicators (wind speed ratio and snow mass flux ratio) for various input conditions (topography, wind speed and direction, snowfall converted to the precipitation rate, height and density of the shelterbelt, and the presence of auxiliary fences) for the simulations of blowing and drifting snow. Here, the ΣPAD at a given height is used as a value that takes into consideration the shelterbelt width, the degree of leaves and branches. We selected the three survey lines shown in Table 3 and survey line A-1 to examine the effectiveness of the auxiliary fence and created a set of benchmark data with which to examine the calculation conditions that could be generally reproduced by a simulation of blowing and drifting snow using elements on these lines as input conditions (Figure 7).

Table 3: Survey lines used to generate the benchmark data.

| investigated items | Line | Indicators | | Utilization of the benchmark data in examining the setting conditions for simulations |
|---|---|---|---|---|
| | | Wind speed ratio | Snow mass flux ratio | |
| Relationship between indicators and ΣPAD | B-3 | ○ | | Examining the setting conditions based on the reproduction of the relationship between the shelterbelt conditions and the snowbreak performance of that shelterbelt |
| | A-2 | ○ | ○ | |
| | A-3 | ○ | ○ | |
| With versus without an auxiliary fence | A-1 | ○ | | Assessing reproducibility based on the conditions with versus without an auxiliary fence |

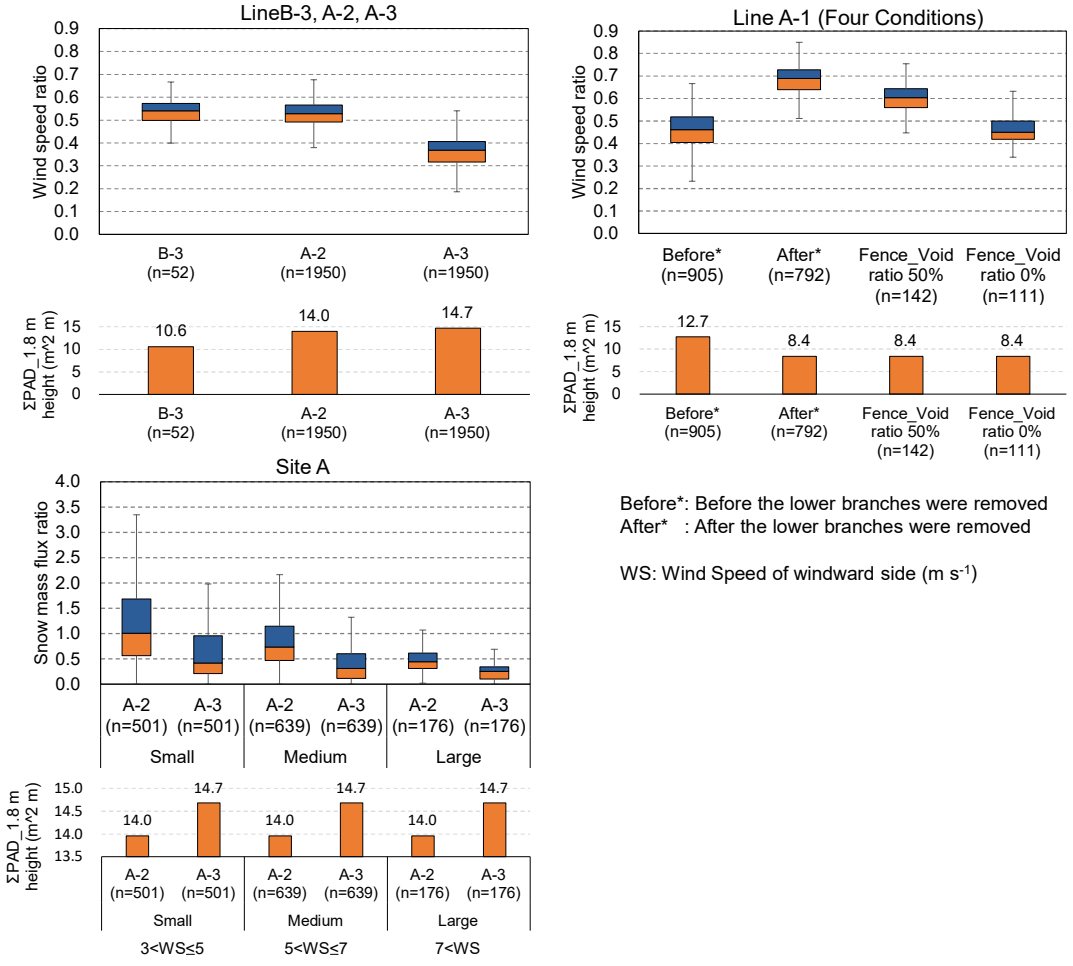


Figure 7: Benchmark data (wind speed ratio vs. ΣPAD, snow mass flux ratio vs. ΣPAD)

## 4. FUTURE STUDIES

In this paper, we analyzed field observation data for two winters, focusing on evergreen conifers and on conditions with versus without an auxiliary fence, and we created benchmark data based on the relationship between the ΣPAD and the wind speed ratio and snow mass flux ratio. Based on the generated benchmark data, we will consider the optimal calculation conditions (mainly, the boundary conditions and models) for numerical simulations of blowing and drifting snow. Then, we will conduct numerical simulation experiments that take into consideration the ΣPAD that is assumable for LSF growth models in order to derive a model for evaluating an LSF's performance. (Figure 9). Using the derived model for an LSF's performance, we will propose structures for LSFs that afford optimal performance in severe blowing and drifting snow.

## REFERENCES


Bouvier, M., S. Durrieu, R. A. Fournier, and R. Jean-Pierre: Generalizing predictive models of forest inventory attributes using an area-based approach with airborne las data. Remote Sensing of Environment, 156, 322-334, http://doi.org/10.1016/j.rse.2014.10.004, 2015.

Civil Engineering Research Institute for Cold Region (CERI): The highway snowstorm countermeasure manual (Revised Edition 2011). Published by CERI, Public Works Research Institute, Incorporated Administrative Agency, 2011.

GitHub – r-lidar/lidR: Airborne LiDAR data manipulation and visualization for forestry application, https://github.com/r-lidar/lidR

Goodison, B.E., P.Y.T. Louie, and D. Yang: WMO Solid Precipitation Measurement Intercomparison Final Report, WMO, WMO/TD-No.872, Instruments and Observing Methods Report No.67, 212 pp, 1998.

Harada, Y., A. Yoshii, S. Omiya, and A. Nishimura: Observations and analysis to develop performance requirements for a Living Snow Fence during severe snowstorm events, Proceedings of the International Snow Science Workshop, Bend, OR, 8-13 October 2023, 2023.

R Development Core Team: R: A language and environment for statistical computing. R Foundation for Statistical Computing, Vienna, Austria, 2004.

Sakurai, T., T. Matsushima, Y. Harada, and A. Nishimura: Windspeed reduction at a living snow fence along a national highway estimated using optical porosity as the index, Proceedings of the XXVIIth World Road Congress (PIARC), IP0123, 1-11, 2023.


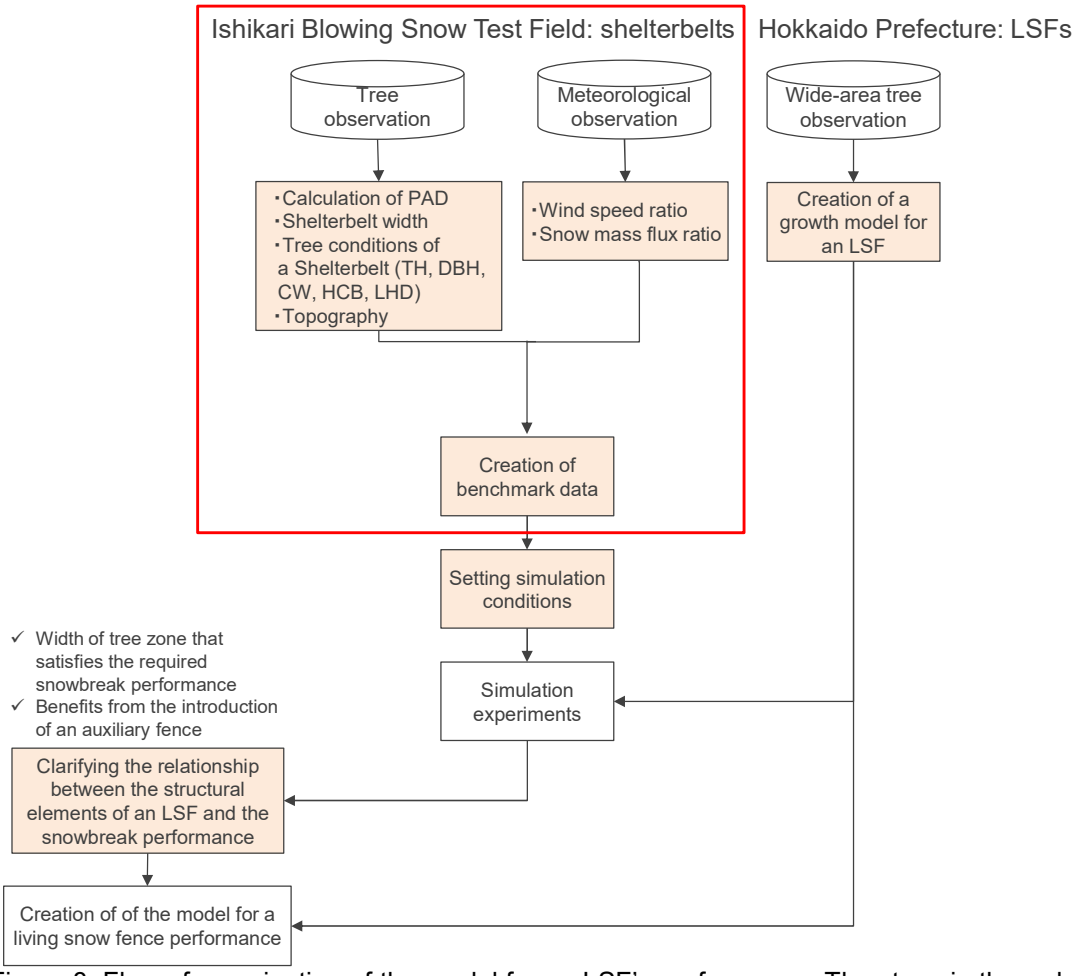


Figure 8: Flow of examination of the model for an LSF's performance. The steps in the red square are the procedures that were examined in this study.